

Spatially Resolved Tracer Diffusion in Complex Responsive Hydrogels

Swen Lehmann,[†] Sebastian Seiffert,^{‡,§} and Walter Richtering^{*,†}

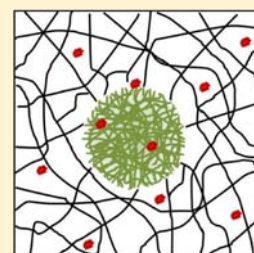
[†]Institute of Physical Chemistry, RWTH Aachen University, Landoltweg 2, D-52074 Aachen, Germany

[‡]F-12 Soft Matter and Functional Materials, Helmholtz-Zentrum Berlin, Hahn-Meitner-Platz 1, D-14109 Berlin, Germany

[§]Institute of Chemistry and Biochemistry, FU Berlin, Takustr. 3, D-14195 Berlin, Germany

S Supporting Information

ABSTRACT: Thermosensitive composite hydrogels that consist of a poly(acrylamide) hydrogel matrix with embedded micrometer-sized poly(*N*-isopropylacrylamide) microgel beads are promising models for complex, heterogeneous gels. We investigate the coupling of the microgel beads with the gel matrix and the formation of interpenetrating networks inside the microgels by confocal two-focus fluorescence correlation spectroscopy (2fFCS). This technique serves to study the effects of the heterogeneous structure of the composite hydrogels on the diffusive mobility of nanoscopic dextran tracers within the gels. Our investigations reveal that the formation of interpenetrating networks inside the embedded microgel beads depends on their cross-link density: whereas interpenetrating networks are formed inside weakly cross-linked beads, they are not formed inside strongly cross-linked beads. If the formation of interpenetrating networks occurs, the temperature-dependent swelling and deswelling of the beads is obstructed. In addition, the mobility of dextran tracers inside the embedded microgel beads is hindered compared to those in free beads and in the surrounding gel matrix. Surprisingly, the surrounding poly(acrylamide) hydrogel matrix swells inhomogeneously when the embedded poly(*N*-isopropylacrylamide) beads collapse upon heating. This indicates the formation of pores near the surface of the collapsed beads, offering promising means to tailor composite hydrogels for applications as membranes with tunable permeability. Our experiments also demonstrate the utility of 2fFCS to study spatially resolved diffusion in complex environments, which is of great interest in biomaterials research.



INTRODUCTION

Hydrogels are highly hydrated, cross-linked polymer networks that are valuable for many biological applications,^{1,2} including those in drug delivery,^{3–5} biosensing,⁶ and tissue engineering.^{7–11} In one class of applications, hydrogels serve as scaffolds for the encapsulation of living cells.¹² Such systems provide a versatile platform to study the interaction of cells with confining environments that exhibit mechanical characteristics similar to that of the cells. A particularly important technique to be used in this context is traction force microscopy.¹³ In this approach, cells are imbedded into a hydrogel along with colloidal tracer particles. Tracking the displacements of these particles serves to measure the traction forces that the encapsulated cells exert on their environment in response to external stimuli. These studies provide a basis to understanding the complex relationship between cells and physiological environments, which is a crucial step toward understanding physiological processes such as cell migration, tissue morphogenesis, and signaling pathways.¹³

The use of cell-laden hydrogels in traction force experiments requires sound knowledge on the micro- and nanostructural complexity of the gel environment close to the encapsulated cells. In addition, it is necessary to understand the dynamics of additives such as cell nutrition and signaling compounds inside these systems, because this affects the viability and ability of the encapsulated cells to communicate and to be stimulated.

To acquire such knowledge, it is helpful to perform investigations on model systems that are less complex and provide more flexibility for custom variation of experimental parameters than real cell-laden gels. For this purpose, composite gels that consist of micrometer-sized hydrogel particles embedded into a surrounding independent hydrogel matrix are of particular value.^{14–16} If the embedded microgel particles are built from environmentally sensitive polymers¹⁷ that can react to changes in their surrounding by pronounced swelling and deswelling, they provide a perfect model for cells that contract or relax upon stimulation.¹⁸

To ascertain the utility of microgel-laden, composite gel systems as models for more complex cell-laden gels, it must be known to what extent the presence of the external scaffolding gel matrix affects the ability of the embedded microgels to swell and deswell. Conversely, it must also be known how the swelling and deswelling of the embedded microgels affects and distorts the surrounding scaffolding gel. Previous work by our group has shown that the incorporation of environmentally responsive microgels into a scaffolding gel matrix retains the sensitivity the embedded microgels. For example, the size of poly(*N*-isopropylacrylamide) (PNIPAM) microgel particles embedded into a scaffolding poly(acrylamide) (PAAM) gel matrix has the same temperature dependence as in plain

Received: July 12, 2012

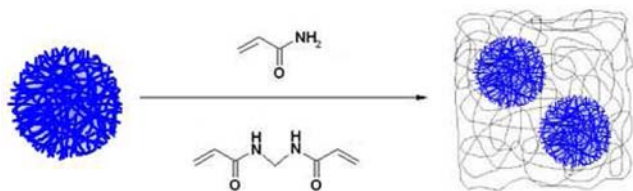
Published: August 31, 2012

aqueous environment.^{15,19} Moreover, when these particles undergo their volume-phase transition, the size and shape of the entire composite system remains unaffected; this is because the gel matrix takes up the water that is released by the embedded microgels.²⁰

These observations suggest that the sensitive microgels are embedded freely into the scaffolding gel matrix, without formation of an interpenetrating network. However, large microgel beads might behave differently due to their different internal structure as compared to small microgels.²¹ Thus, knowledge about the presence or absence of interpenetrating network domains in composite gel matrixes filled with large microgel beads is crucial to appraise their utility as model systems for more complex, cell-laden gels. In addition, no previous work has yet focused on using composite gels to investigate the influence of heterogeneous structures on the local, spatially resolved dynamics of nano- and mesoscopic probe molecules that move through the hydrogel. The derivation of a sound knowledge on the tracer mobility in these complex environments is another precondition to ascertain the utility of composite gels as models for cell-laden gels. This knowledge is also of direct relevance to understand the viability and reactivity of cells that are immobilized in hydrogel matrixes.^{12,22}

In this paper, we use composite hydrogels that consist of micrometer-sized, thermosensitive microgel particles (labeled with a fluorescent dye) embedded into a soft hydrogel matrix (see Scheme 1) to study the diffusive mobility of nanometer-

Scheme 1. Illustration of the Formation of Composite Hydrogels That Consist of Micrometer-Sized, Thermoresponsive Microgel Beads Embedded into a Soft Hydrogel Matrix²⁴



sized tracers (labeled with a different fluorescent dye); this is achieved by two-focus fluorescence correlation spectroscopy (2fFCS).²³ In addition, we use these composites to study the interplay of the embedded microgel particles with the surrounding scaffolding gel matrix to unravel the presence or absence of interpenetrating polymer network structures within the microgel beads. This is achieved by observing the swelling and deswelling of the thermosensitive microgel beads within the scaffolding hydrogel matrixes through the use of confocal laser scanning microscopy.

EXPERIMENTAL SECTION

Sample Preparation. Fluorescently labeled PNIPAM microgel beads were prepared from *N*-isopropylacrylamide (NIPAM, Acros Organics), BIS, and methacryloyloxyethyl thiocarbonyl rhodamine B (Polysciences Inc.) in two different ways: type-A beads (cross-linker to monomer ratio, 1:70; PNIPAM concentration, 100 g L⁻¹) were fabricated by droplet-based microfluidic templating,²⁵ whereas type-B beads (cross-linker to monomer ratio, 1:13; PNIPAM concentration, 143 g L⁻¹) were synthesized by inverse suspension polymerization.²⁶

Dextran labeled with Alexa Fluor 647 (10 kDa and 3 kDa, Invitrogen) or Alexa Fluor 488 (70 kDa, Invitrogen) were dissolved in

water (LiChroSolv, Merk). Dextran with a mass of 3 kDa has a hydrodynamic radius of $R_h = 1$ nm, 10 kDa dextran has $R_h = 2.3$ nm, and 70 kDa dextran has $R_h = 6.5$ nm. All hydrodynamic radii were calculated via the Stokes–Einstein equation from the diffusion coefficient measured at infinite dilution.

Composite hydrogel samples were prepared with a final bead volume fraction of 0.05 at 25 °C (see Table 1). Less than 1 mg of the

Table 1. Compositions of Composite Hydrogel Samples That Consist of PNIPAM Microgel Beads Embedded within PAAM Hydrogel Matrixes^a

sample name	c_{PAAM} (g L ⁻¹)	c_{PNIPAM} (g L ⁻¹)	$n_{\text{BIS}}/n_{\text{PAAM}}$	$n_{\text{BIS}}/n_{\text{PNIPAM}}$
HG-25-A	25	100	1:60	1:70
HG-50-A	50	100	1:60	1:70
HG-25-B	25	143	1:60	1:13
HG-50-B	50	143	1:60	1:13

^aHG in the sample name indicates the existence of a PAAM hydrogel; 25 or 50 indicates the PAAM concentration in the hydrogel; A and B denote the bead type; c_{PAAM} is the matrix concentration; c_{PNIPAM} the PNIPAM concentration during bead preparation; $n_{\text{BIS}}/n_{\text{PAAM}}$ is the molar ratio of cross-linker to monomer in the matrix; $n_{\text{BIS}}/n_{\text{PNIPAM}}$ is the molar ratio of cross-linker to monomer in the beads.

UV-cleavable initiator VA-086 (2,2'-azobis[2-methyl-*N*-2-hydroxyethyl)propionamide], Wako) was added, and the solutions were filled into a temperature-controlled sample cell.²⁷ The polymerization was performed under UV exposure with an intensity of 1.5 W cm⁻² at $\lambda = 254$ nm for 30 min at 25 °C after mixing the stock solutions.

All the bead particles, the hydrogels, and the composite gels were synthesized at 25 °C. In this state, monomers and cross-linkers are homogeneously distributed in the pregel reaction mixtures, which lead to a rather uniform distribution of cross-linker in the hydrogel. Thus, we assume that gel matrix and gel beads exhibit similar spatial distribution of cross-links.

Note that the type-A beads are less cross-linked and contain less polymer than the type-B beads. Hence, the type-A beads are referred to as soft beads, whereas the type-B beads are referred to as dense beads.

Dynamic Light Scattering. Dynamic light scattering (DLS) experiments are performed to determine the mesh size of the gels. We use an ALV DLS with a 7004 correlator (ALV-Laser Vertriebgesellschaft m-b.H., Langen, Germany), equipped with a 473 nm, 40 mW DPSS laser (Cobold AB, Sweden). As gels are nonergodic, we used the Pusey–van Megen method to determine the mesh size of our gel samples.²⁸ To determine the mesh size of the PNIPAM beads, we synthesize macroscopic hydrogels with the same composition at comparable reaction conditions.

The mesh size of a PAAM hydrogel with a composition of 50 g L⁻¹ of PAAM and $n_{\text{BIS}}/n_{\text{PAAM}}$ of 1:60 at 25 °C is in the order of 15 nm, whereas the mesh size of a PNIPAM hydrogel with a composition of 100 g L⁻¹ of PNIPAM and $n_{\text{BIS}}/n_{\text{PNIPAM}}$ of 1:70 at 25 °C is in the order of 19 nm.

Spatially Resolved 2fFCS. Fluorescence correlation spectroscopy (FCS) is well-suited to measure the diffusion coefficient of tracer particles in gels.^{29,30} In this context, the correct treatment of potential changes in the confocal volume, which can occur due to changes in the sample refractive index, is of major importance.³¹ This is particularly relevant for the present study, because the local polymer density varies with the position in composite gels, leading to different refractive indexes and thus different sizes and shapes of the confocal volume.

To account for these complications, we use 2fFCS.²³ In 2fFCS, two laterally shifted but overlapping laser foci are used to determine correlation functions of each focus and of the cross section of the two foci. The lateral shift is obtained by the use of a Nomarski prism, which leads to the shift distance δ that is not affected by refractive index mismatch and optical saturation.

The correlation function in 2fFCS is given by the following:

$$g(t, \delta, \nu) = \frac{c}{4} \sqrt{\frac{\pi}{Dt}} \int dz_1 \int dz_2 \left(\frac{\kappa(z_1)\kappa(z_2)}{8Dt + w^2(z_1) + w^2(z_2)} \right) \times \exp \left[-\frac{(z_2 - z_1 - \nu_z t)^2}{4Dt} - 2 \frac{(\delta - \nu_x t)^2 + \nu_y^2 t^2}{8Dt + w^2(z_1) + w^2(z_2)} \right] \quad (1)$$

In eq 1, D is the translational diffusion coefficient, t the lag time of the correlation, c the concentration of the fluorescent particles, δ is the shift distance (determined independently), and x , y , and z are Cartesian coordinates with z along the optical axis. ν_i are optical fit parameters including the fluorescence excitation efficiency and quantum yield.

$$w(z) = w_0 \left[1 + \left(\frac{\lambda_{\text{ex}} z}{\pi w_0^2 n} \right)^2 \right]^{1/2} \quad (2)$$

$$\kappa(z) = 2 \int_0^a \frac{d\rho\rho}{R^2(z)} \exp \left(-\frac{2\rho^2}{R^2(z)} \right) = 1 - \exp \left(-\frac{2a^2}{R^2(z)} \right) \quad (3)$$

$$R(z) = R_0 \left[1 + \left(\frac{\lambda_{\text{em}} z}{\pi R_0^2 n} \right)^2 \right]^{1/2} \quad (4)$$

λ_{ex} is the excitation wavelength, λ_{em} is the emission wavelength, n the refractive index, and a is the confocal pinhole radius. The correlation function can be calculated numerically, and w_0 and R_0 are fit parameters.³² The high accuracy of 2fFCS in crowded environments has been demonstrated previously.³³

Tracer diffusion measurements in pure PAAM hydrogels are performed at nine different positions, each yielding the same diffusion coefficient. This shows that 2fFCS probes diffusion processes on length scales larger than spatial heterogeneities within the hydrogels.^{34,35}

To achieve high spatial resolution for tracer diffusion experiments in 2fFCS, we employ a confocal microscope. A three-dimensional (3D) piezo table with a range of 100 μm in all three directions serves to locate the regions of interest. With this setup, we measure the diffusion coefficient at several defined points in the sample. Measurements inside microgel beads at 36 $^\circ\text{C}$ are precluded due to the high scattering intensity caused by the collapsed particles. Similar effects were reported by Raccis et al. for the diffusion of dyes in collapsed PNIPAM hydrogels.³⁰

A typical measurement time is 1 h. The error bars for the diffusion coefficients obtained in spatially resolved measurements are obtained from fits of the correlation function.

RESULTS AND DISCUSSION

PNIPAM microgels show pronounced swelling and deswelling upon changes in temperature; this transition is accompanied by microgel volume changes of up to 1000%.³⁶ The swellability of these and other microgel particles depends on the cross-link density of their constituent polymer network. The swellability of the PNIPAM microgel beads to be used in this work is characterized by their temperature-dependent sizes prior to their incorporation into a hydrogel matrix; this is determined by fluorescence microscopy. Fluorescence micrographs recorded at 25 and 36 $^\circ\text{C}$ show that soft, loosely cross-linked microgel beads, hereinafter referred to as “type-A beads”, deswell with $\Delta V = V_c/V_s = (R_c/R_s)^3 = 0.09 \pm 0.01$, whereas stiff, densely cross-linked beads, hereinafter referred to as “type-B beads”, deswell with $\Delta V = 0.42 \pm 0.15$, (Supporting

Information, Figure S1). Here, ΔV is the ratio of the microgel volume in the collapsed state, V_c , and the microgel volume in swollen state, V_s . R_c and R_s are the corresponding microgel particle radii.

If these microgels are embedded into surrounding 50 g L^{-1} PAAM hydrogel matrixes, the less cross-linked, soft type-A beads (HG-50-A) collapse ($\Delta V = 0.61$) much less upon heating as compared to their behavior in water ($\Delta V = 0.09$), as shown in Figure 1. This can be explained by the formation of a PAAM

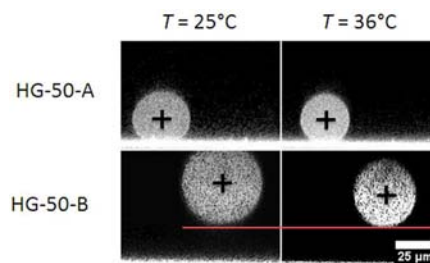


Figure 1. Side view of PNIPAM beads embedded in a PAAM hydrogel with an AAM concentration of 50 g L^{-1} . The white line at the bottom of the pictures is the glass cover slide. The beads are scanned in the center plane of the particle along the x – z directions (Supporting Information, Figure S2). Top: PNIPAM bead of type A at 25 $^\circ\text{C}$ (left) and at 36 $^\circ\text{C}$ (right). The bead collapse is much less pronounced than in water. Bottom: PNIPAM bead of type B at 25 $^\circ\text{C}$ (left) and at 36 $^\circ\text{C}$ (right). The bead collapses as in water, and the center of the bead moves down until the collapsed bead reaches the level of the bottom of the swollen bead. Black crosses indicate the center of the beads. The scale bar denotes 25 μm and applies to all panels.

gel inside the beads that interpenetrates the gel–bead PNIPAM gel network, thereby obstructing the thermo-induced collapse of the beads. By contrast, the dense type-B beads (sample HG-50-B) collapse just as they do in water, as also shown in Figure 1. This indicates that their dense structure prevents the formation of an interpenetrating gel.

Figure 1 also shows that the center of mass of the type-B beads moves downward when these beads collapse. Again, this indicates that there is hardly any coupling between the type-B beads to the surrounding hydrogel matrix.

When the segmental density of the PAAM matrix is lowered to only 25 g L^{-1} (sample HG-25-A), a different result is obtained: in this case, the soft type-A beads *do* collapse inside the PAAM matrix just as they do in water, as shown in Figure 2. In this sample, however, the center of the bead does *not* move when the bead collapses, which is different from the behavior of the highly cross-linked beads in sample HG-50-B, which collapse and move downward upon heating. This marked

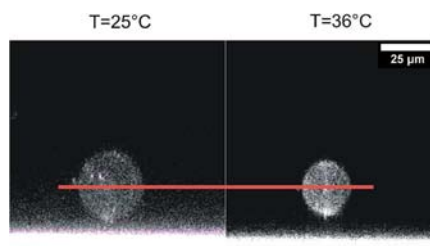


Figure 2. Side view of type-A PNIPAM bead embedded in a PAAM hydrogel with an AAM concentration of 25 g L^{-1} . The bead collapses almost to the same extent as in water, and the bead center does not move. The scale bar denotes 25 μm and applies to both panels.

difference is an indication for the formation of an interpenetrating network that is not strong enough to prevent bead collapse but still strong enough to keep the bead at its position upon heating.

The previous experiments demonstrate how the coupling with a surrounding gel matrix influences the temperature-sensitive swelling of hydrogel-embedded microgel beads. To supplement a nanometer-scale picture, we now turn to the molecular scale and discuss the influence of this coupling on the mobility of molecules that diffuse through these gels. In particular, we investigate how the heterogeneous local environment affects the mobility of these probe molecules. We use fluorescently labeled dextrans as tracer particles; these tracers hardly interact with other molecules³⁷ and have therefore been employed in related previous investigations.^{38–41} We quantify the dextran diffusivity inside the microgel beads and outside of them in the surrounding hydrogel matrix by 2fFCS.

The diffusion of 10 kDa dextran is slower inside the water-swollen type-A PNIPAM beads than it is in pure water, as illustrated in Figure 3 (open symbols). The diffusivities inside

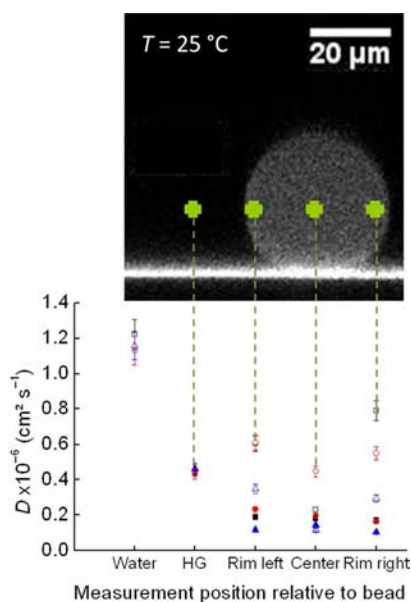


Figure 3. Diffusion coefficient of 10 kDa dextran out and inside of type-A PNIPAM microgel beads, either embedded into a 25 g L⁻¹ PAAM hydrogel matrix (filled symbols) or suspended in water (open symbols). The upper picture is a confocal micrograph showing the different positions of measurement. $T = 25 \text{ }^\circ\text{C}$. Different symbols (triangles, squares, and circles) indicate measurements performed on different beads. For 3 kDa dextran, see the Supporting Information, Figure S4.

the beads agree well with those in macroscopic PNIPAM hydrogels of the same composition. This finding suggests that the gel architecture inside the type-A microgels resembles that inside a bulk macroscopic gel. This appears justified, because these beads were templated in emulsion droplets that solely act as micrometer-sized reaction vessels without any impact on the course of the free-radical polymer network formation.

The tracer diffusion inside the water-swollen beads depends slightly on the position of measurement. The tracer diffusion coefficient determined in the center of the bead is lower than that determined near to the bead surface. This is surprising, as it is expected that beads prepared in the swollen state have a

homogeneous cross-link density. We address this finding to the circumstance that, when dissolved in water, the beads swell a little compared to the size during their polymerization. Our spatially resolved tracer diffusion experiments indicate that this swelling is not fully affine.

Corresponding investigations on a composite gel with a matrix concentration of 25 g L⁻¹ that is loaded with the same type-A microgel beads show that the tracer diffusion inside the embedded beads is slower as compared to both the diffusion in beads dissolved in water and to the diffusion in the surrounding PAAM hydrogel matrix (Supporting Information, Figure S3), as shown in Figure 3 (filled symbols). This finding indicates that an interpenetrating network has formed inside the beads.

Increase of the concentration of PAAM in the surrounding hydrogel matrix pronounces the effect of tracer deceleration inside the microgel beads: if the same experiments are repeated at a PAAM concentration of 50 g L⁻¹, the dextran tracer diffusion coefficient inside the embedded bead is reduced further; it is also again lower as compared to the hydrogel matrix and the free bead in pure water, as shown in Figure 4.

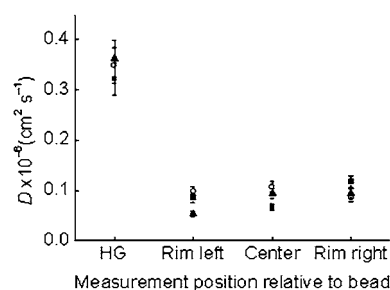


Figure 4. Diffusion coefficient of 10 kDa dextran out and inside of type-A PNIPAM microgel beads embedded into a 50 g L⁻¹ PAAM hydrogel matrix. $T = 25 \text{ }^\circ\text{C}$. Different symbols (triangles, squares, and circles) indicate measurements on different beads.

The diffusion of tracers through a gel depends on the mesh size of the constituent polymer network relative to the size of the tracer.⁴² The mesh size of PAAM gels at 50 g L⁻¹ and different cross-linker ratios can be determined by dynamic light scattering. We follow this approach and determine it to be in the order of 15 nm, in good agreement with literature data.⁴³ The hydrodynamic diameter of 10 kDa dextran in water is 4.6 nm; this is rather small compared to the polymer network mesh size. We describe the diffusion coefficient of the tracer as

$$D = \frac{kT}{f_{\text{eff}}} \quad (5)$$

where kT is the thermal energy and f_{eff} is an effective friction coefficient. In this approach, the hydrogel is considered as a continuous environment providing an effective friction for the random motion of the tracer on the length scale probed by FCS.⁴⁴

Hydrogels are known to exhibit heterogeneities on length scales of 10–100 nm.^{34,35} This is smaller than the optical resolution of our 2fFCS measurements, which probes the mobility of labeled molecules on length scales that are limited by the optical resolution. The shift distance between the two foci in our 2fFCS setup is of the order >300 nm. Thus, the mobility of tracer molecules probed by 2fFCS is averaged over both mesh size fluctuations and heterogeneities.

The two-foci cross-correlation data acquired in this study can all be fitted to eq 1 (Supporting Information, Figure S5). Thus, we do not observe anomalous diffusion.

Table 2 summarizes the diffusion coefficients of the 10 kDa tracer in different environments. Dividing the diffusion

Table 2. Diffusivities and Relative Friction Coefficients of 10 kDa Dextran Tracers That Diffuse through PNIPAM–PAAM Composite Gel Matrixes at 25 °C

medium	D (10^{-6} cm 2 s $^{-1}$)	f_{eff}
water	1.17	----
bead A	0.443	2.6
HG-25	0.449	2.6
HG-50	0.344	3.4
HG-25-A	0.167	7
HG-50-A	0.089	13

coefficient in water (D_w) by the diffusion coefficient in a complex environment (PNIPAM bead or PAAM matrix plus embedded bead, respectively) yields the effective friction coefficient of the tracer inside this environment relative to that in water.

The data in Table 2 show that the increased friction encountered by the 10 kDa dextran tracers inside the embedded microgel beads in sample HG-25-A ($f_{\text{eff}} = 7$) can be approximated by a sum of the friction coefficients of the beads ($f_{\text{eff}} = 2.6$) and the gel matrix ($f_{\text{eff}} = 2.6$). However, in the case of sample HG-50-A, the experimental friction coefficient ($f_{\text{eff}} = 13$) is much higher and cannot be modeled by simple addition of the bead ($f_{\text{eff}} = 2.6$) and gel ($f_{\text{eff}} = 3.4$) friction contributions. This indicates that the effective mesh size of the interpenetrating network inside the beads in sample HG-50-A is no longer large compared to the size of the tracer; thus, the topological restrictions of the network affect the tracer diffusion in this case.

Finally, we address the question whether the formation of interpenetrating networks and potential bead collapse also affect the tracer diffusion within the surrounding hydrogel matrix *outside* the beads. For this purpose, we probe the diffusion coefficients of 3 and 70 kDa dextrans in the hydrogel matrixes at 25 and 36 °C with samples HG-25-A and HG-25-B. At 25 °C, which corresponds to the preparation temperature of the pure PAAM gel and the two composite gels HG-25-A and HG-25-B, we find identical tracer diffusion coefficients in the matrix. This is expected and demonstrates that the incorporation of the microgel beads does not affect the formation of the PAAM gel.

Figure 5 displays the diffusion coefficient of 70 kDa dextran in the hydrogel matrix of sample HG-25-A. In this plot, the diffusion coefficient is normalized by the solvent viscosity, η , and by the temperature, T , to account for the trivial temperature dependence of diffusion. The normalized diffusion coefficients do not change when the sample is heated from 25 to 36 °C, and there is no dependence on the distance to the bead surface. For this sample, we have shown that an interpenetrating network is formed. However, the collapse of the bead does not affect the tracer diffusion in the surrounding matrix. The same result is found for 3 kDa dextran in this sample (Supporting Information, Figure S6).

In contrast to the presence of an interpenetrating network in sample HG-25-A, there are no indications for an interpenetrating network in sample HG-25-B. The normalized

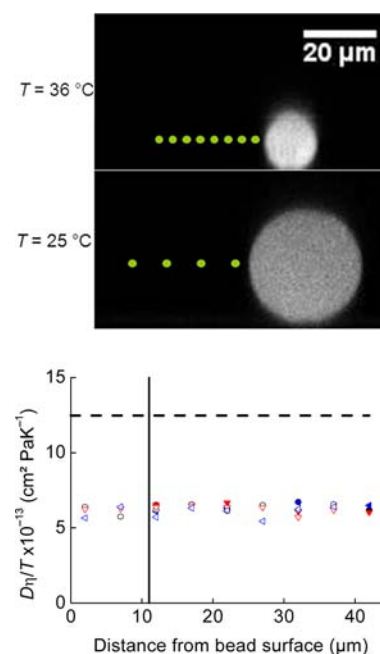


Figure 5. Normalized diffusion coefficients of 70 kDa dextran in the hydrogel matrix close to the bead surface in sample HG-25-A. Full symbols denote $T = 25$ °C, whereas open symbols denote $T = 36$ °C. Measurements were conducted on three different beads, as represented by different symbols (circles, upright triangles, and inverted triangles). The dashed line indicates the normalized diffusion coefficients of 70 kDa dextran in water. The vertical solid line indicates the position of the bead surface at $T = 25$ °C.

tracer diffusion coefficients in the gel matrix of this sample are enhanced near the particle surface upon heating, as shown in Figure 6. We address this finding to the following rationale:

The data at 25 °C are taken at positions outside the beads, and when these positions are studied at 36 °C, the diffusion coefficient, normalized by the change of η and T , is not affected. Due to the strong collapse of the beads, however, it is possible to measure tracer diffusivities at positions that were occupied by the bead at 25 °C but are no longer occupied at 36 °C, as represented by the 36 °C data left of the vertical line in Figure 6. These tests show that the tracer diffusivity *increases* in the volume formerly occupied by the bead when the bead is deswollen at 36 °C (measurements near the bead surface were performed after annealing times of 7 h to ensure that the hydrogel matrix has enough time to reach equilibrium swelling). The value of the increased normalized diffusion coefficient of 3 kDa dextran is the same as in water at 36 °C (Figure 6, center). This suggests that the PAAM hydrogel is locally swollen so much by the water released from the collapsed bead that the small 3 kDa dextran is no longer restricted in its diffusion. The 70 kDa dextran also shows accelerated diffusion inside the volume previously occupied by the beads (Figure 6, bottom). However, the normalized diffusion is always smaller than in water.

These results show that the PAAM hydrogel matrix has swollen into the volume that was formerly occupied by the bead at 25 °C. The local segmental density of the PAAM hydrogel in these regions is lower than that in the bulk gel away from the bead, indicating that the gel matrix swells heterogeneously. The segmental density is still sufficiently high to hinder the diffusion of 70 kDa dextran compared to its diffusion in pure water, but the gel does no longer obstruct the

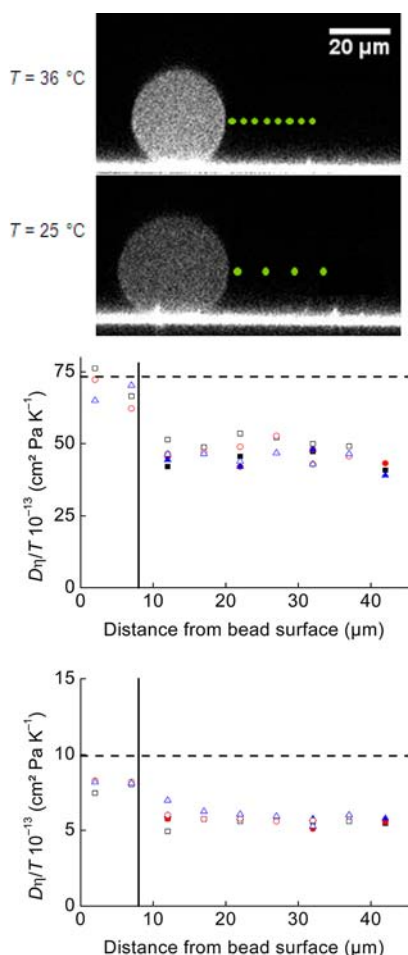


Figure 6. Normalized diffusion coefficients of 3 kDa dextran (center) and 70 kDa dextran (bottom) in the hydrogel matrix close to the bead surface in sample HG-25-B. Full symbols denote $T = 25$ °C, whereas open symbols denote $T = 36$ °C. Measurements were conducted on three different beads, as represented by different symbols (squares, circles, and triangles). The dashed lines indicate the normalized diffusion coefficients of the dextrans in water. The vertical solid line indicates the position of the bead surface at $T = 25$ °C. The scale bar denotes $20 \mu\text{m}$ and applies to both panels.

diffusion of 3 kDa dextran. As the swelling of the matrix is localized to the volume close to the beads, it might be possible to form channels across the composite hydrogel when the bead concentration is so high that the beads are close together in the swollen state but apart from each other at higher temperatures when they are deswollen.

CONCLUSIONS

Interpenetrating polymer networks can be formed in composite hydrogels that consist of microgel particles embedded in a surrounding macroscopic gel matrix. However, this depends on the density of the embedded microgel beads. No interpenetrating networks are formed inside the incorporated beads when the beads are highly cross-linked. In this limit, spatially resolved tracer diffusion measurements reveal that the hydrogel matrix swells heterogeneously when the beads collapse, indicating the formation of pores near their surface.

By contrast, interpenetrating networks are found with less cross-linked beads; this entails slower diffusion of tracers inside the beads. In this scenario, the temperature-dependent swelling

of the PNIPAM beads depends on the polymer concentration of the hydrogel matrix.

These results show that the properties of thermosensitive composite hydrogels as well as the mobility of guest species can be tailored by the composition of the embedded particles and the surrounding gel matrix. Tuning these parameters can therefore serve to control the movement of active species through such composite hydrogels. This foreshadows the utility of these systems as membranes with tunable permeability in separation techniques and analytical sciences. In addition, our experiments demonstrate the utility of 2fFCS for the determination of spatially resolved tracer diffusion in complex gels or biomaterials.

ASSOCIATED CONTENT

Supporting Information

Additional diffusion coefficient data of the responsive composite gels, pure PAAM gels, 2fFCS correlation functions, fluorescent microscopy images of the microgel beads dispersed in water, and a schematic drawing of the filled hydrogels. This material is available free of charge via the Internet at <http://pubs.acs.org>.

AUTHOR INFORMATION

Corresponding Author

richtering@rwth-aachen.de

Notes

The authors declare no competing financial interest.

ACKNOWLEDGMENTS

We thank Judith Meid for preparing type-B PNIPAM beads. We also thank the Deutsche Forschungsgemeinschaft for financial support within SPP 1259. S.S. is a Liebig fellow of the Fund of the Chemical Industry (Germany) and acknowledges funding by the Focus Area NanoScale at FU Berlin.

REFERENCES

- (1) Xu, X.; Jha, A. K.; Harrington, D. A.; Farach-Carson, M. C.; Jia, X. *Soft Matter* **2012**, *8*, 3280–3294.
- (2) Kuckling, D. *Colloid Polym. Sci.* **2009**, *287*, 881–891.
- (3) Sivakumaran, D.; Maitland, D.; Hoare, T. *Biomacromolecules* **2011**, *12*, 4112–4120.
- (4) Gurski, L. A.; Jha, A. K.; Zhang, C.; Jia, X. Q.; Farach-Carson, M. C. *Biomaterials* **2009**, *30*, 6076–6085.
- (5) McGillicuddy, F. C.; Lynch, L.; Rochev, Y. A.; Burke, M.; Dawson, K. A.; Gallagher, W. M.; Keenan, A. K. *J. Biomed. Mater. Res., Part A* **2006**, *79A*, 923–933.
- (6) Jonas, U.; Mateescu, A. *Polym. Prepr. (Am. Chem. Soc., Div. Polym. Chem.)* **2012**, *53*, 297–298.
- (7) Tumarkin, E.; Tzadu, L.; Cszasz, E.; Seo, M.; Zhang, H.; Lee, A.; Peerani, R.; Purpura, K.; Zandstra, P. W.; Kumacheva, E. *Integr. Biol.* **2011**, *3*, 653–662.
- (8) Cohen Stuart, M. A.; Huck, W. T. S.; Genzer, J.; Mueller, M.; Ober, C.; Stamm, M.; Sukhorukov, G. B.; Szleifer, I.; Tsukruk, V. V.; Urban, M.; Winnik, F.; Zauscher, S.; Luzinov, I.; Minko, S. *Nat. Mater.* **2010**, *9*, 101–113.
- (9) Langer, R.; Vacanti, J. P. *Science* **1993**, *260*, 920–926.
- (10) Dong, Y. X.; Hassan, W.; Zheng, Y.; Saeed, A. O.; Cao, H. L.; Tai, H. Y.; Pandit, A.; Wang, W. X. *J. Mater. Sci.: Mater. Med.* **2012**, *23*, 25–35.
- (11) Nakajima, T.; Kurokawa, T.; Furukawa, H.; Yu, Q. M.; Tanaka, Y.; Osada, Y.; Gong, J. P. *Chin. J. Polym. Sci.* **2009**, *27*, 1–9.
- (12) Velasco, D.; Tumarkin, E.; Kumacheva, E. *Small* **2012**, *8*, 1633–1642.

- (13) Legant, W. R.; Miller, J. S.; Blakely, B. L.; Cohen, D. M.; Genin, G. M.; Chen, C. S. *Nat. Methods* **2010**, *7*, 969–971.
- (14) Salvati, A.; Soderman, O.; Lynch, I. J. *Phys. Chem. B* **2007**, *111*, 7367–7376.
- (15) Musch, J.; Schneider, S.; Lindner, P.; Richtering, W. *J. Phys. Chem. B* **2008**, *112*, 6309–6314.
- (16) Lynch, I.; Dawson, K. A. *J. Phys. Chem. B* **2003**, *107*, 9629–9637.
- (17) Pelton, R. *Adv. Colloid Interface Sci.* **2000**, *85*, 1–33.
- (18) Raz, N.; Li, J. K.; Fiddes, L. K.; Tumarkin, E.; Walker, G. C.; Kumacheva, E. *Macromolecules* **2010**, *43*, 7277–7281.
- (19) Meid, J.; Friedrich, T.; Tieke, B.; Lindner, P.; Richtering, W. *Phys. Chem. Chem. Phys.* **2011**, *13*, 3039–3047.
- (20) Meid, J.; Dierkes, F.; Cui, J.; Messing, R.; Crosby, A. J.; Schmidt, A.; Richtering, W. *Soft Matter* **2012**, *8*, 4354–4263.
- (21) Pich, A.; Richtering, W. *Adv. Polym. Sci.* **2010**, *234*, 1–37.
- (22) Rossow, T.; Heyman, J. A.; Ehrlicher, A. J.; Langhoff, A.; Weitz, D. A.; Haag, R.; Seiffert, S. *J. Am. Chem. Soc.* **2012**, *134*, 4983–4989.
- (23) Dertinger, T.; Pacheco, V.; von der Hocht, I.; Hartmann, R.; Gregor, I.; Enderlein, J. *Chemphyschem* **2007**, *8*, 433–443.
- (24) Soddemann, M. *Lichtstreuung und Rheologie an gefüllten, vernetzten und verzweigten Polymersystemen*. Ph.D. Thesis, Albert-Ludwigs-Universität Freiburg, Freiburg, Germany, November, 18th 2002.
- (25) Seiffert, S. *Macromol. Rapid Commun.* **2011**, *32*, 1600–1609.
- (26) Annaka, M.; Matsuura, T.; Kasai, M.; Nakahira, T.; Hara, Y.; Okano, T. *Biomacromolecules* **2003**, *4*, 395–403.
- (27) Muller, C. B.; Richtering, W. *Colloid Polym. Sci.* **2008**, *286*, 1215–1222.
- (28) Pusey, P. N.; van Megen, W. *Phys. A* **1989**, *157*, 705–41.
- (29) Modesti, G.; Zimmermann, B.; Borsch, M.; Herrmann, A.; Saalwachter, K. *Macromolecules* **2009**, *42*, 4681–4689.
- (30) Raccis, R.; Roskamp, R.; Hopp, I.; Menges, B.; Koynov, K.; Jonas, U.; Knoll, W.; Butt, H. J.; Fytas, G. *Soft Matter* **2011**, *7*, 7042–7053.
- (31) Enderlein, J.; Gregor, I.; Patra, D.; Dertinger, T.; Kaupp, U. B. *Chemphyschem* **2005**, *6*, 2324–2336.
- (32) Muller, C. B.; Loman, A.; Pacheco, V.; Koberling, F.; Willbold, D.; Richtering, W.; Enderlein, J. *Europhys. Lett.* **2008**, *83*, 5.
- (33) Muller, C. B.; Eckert, T.; Loman, A.; Enderlein, J.; Richtering, W. *Soft Matter* **2009**, *5*, 1358–1366.
- (34) Nie, J.; Du, B.; Oppermann, W. *Macromolecules* **2004**, *37*, 6558–6564.
- (35) Shibayama, M. *Macromol. Chem. Phys.* **1998**, *199*, 1–30.
- (36) Schild, H. G. *Macromol. Chem.* **1992**, *3*, 393–395.
- (37) Ponder, E.; Ponder, R. V. *J. Gen. Physiol.* **1960**, *43*, 753–758.
- (38) Vermonden, T.; Jena, S. S.; Barriet, D.; Censi, R.; van der Gucht, J.; Hennink, W. E.; Siegel, R. A. *Macromolecules* **2010**, *43*, 782–789.
- (39) Branco, M. C.; Pochan, D. J.; Wagner, N. J.; Schneider, J. P. *Biomaterials* **2009**, *30*, 1339–1347.
- (40) Al-Baradi, A. M.; Mykhaylyk, O. O.; Blythe, H. J.; Geoghegan, M. *J. Chem. Phys.* **2010**, *134*.
- (41) Seiffert, S.; Oppermann, W. *Polymer* **2008**, *49*, 4115–4126.
- (42) Cheng, Y.; Prud'homme, R. K.; Thomas, J. L. *Macromolecules* **2002**, *35*, 8111–8121.
- (43) Lindemann, B.; Schroder, U. P.; Oppermann, W. *Macromolecules* **1997**, *30*, 4073–4077.
- (44) Enderlein, J. *Phys. Rev. Lett.* **2012**, *108*, 108101/1–108101/4.